JACS
JOURNAL OF THE AMERICAN CHEMICAL SOCIETY
Article
pubs.acs.org/JACS

Facet-Selective Adsorption on Noble Metal Crystals Guided by Electrostatic Potential Surfaces of Aromatic Molecules

Chin-Yi Chiu,[†] Hao Wu,[†] Zhaoying Yao,[†] Fei Zhou,[†] Hua Zhang,[†] Vidvuds Ozolins,[†,‡] and Yu Huang*[,†,‡]

[†]Department of Materials Science and Engineering, University of California, Los Angeles, California 90095, United States
[‡]California NanoSystems Institute, University of California, Los Angeles, California 90095, United States

Supporting Information

ABSTRACT: We aim to provide a model platform composed of aromatic molecules and noble metal surfaces to study the molecular facet-selective adsorption and employ the discoveries to design surfactants for predictable shape-controlled syntheses of nanocrystals. Starting from Pt, it is demonstrated that negative electrostatic potential on the aromatic ring is the prerequisite to display binding selectivity to Pt(111), while a neutral to positive one prefers Pt(100). The geometric matching between molecular binding sites and surface lattices plays a role as well in facet selectivity. Significantly, Raman spectroscopy has been employed to probe the interactions between aromatic molecules and metal surfaces, providing direct evidence of their binding mechanisms. These discoveries are further exploited to design and identify Pd(111) and Pd(100) facet-specific surfactants. These results represent a step forward in achieving predictable and programmable nanostructures through better understanding of organic−inorganic interfaces.

INTRODUCTION

Producing noble metal nanocrystals with well-defined sizes, shapes, and compositions provides an elegant strategy to tune their optical, electronic, and catalytic properties.[1−5] For colloidal nanocrystals, the shape control at the crystallographic level can be achieved through selective adsorption of organic surfactant (or capping agent, ligand) on a particular crystal facet, which modifies its surface energy and alters its growth rate.[6] A variety of organics, such as citric acid, polyvinylpyrrolidone (PVP), and cetrimonium bromide (CTAB), have been recognized as effective surfactants in the shape-controlled syntheses of nanocrystals.[1,7−10] However, the mechanisms regarding their selective adsorption remain elusive, mainly due to the complexity of the synthetic systems and due to the multiple binding or interaction motifs encoded in these molecules.[3,9−11] In addition, understanding the interactions between organic molecules and inorganic surfaces is of paramount importance in catalysis, charge transport at organic−inorganic interface, nanoparticle functionalization, and assembly of nano-objects into ordered or sophisticated structures.[12−16] Surface chemistry of organic molecules on various inorganic surfaces has been extensively studied through experimental techniques and theoretical calculations. Nonetheless, most of the studies were carried out under ultrahigh vacuum, on clean and planar surfaces, with small and simple molecules, such as benzene, and therefore are not directly applicable to more complicated environments (e.g., solutions) and molecules.

Our previous study has demonstrated a rational biomimetic approach to identify the facet-specific peptides which can selectively shape platinum (Pt) nanocrystals during crystal growth in aqueous solution.[17] Specifically, Pt(111) binding peptide (S7) can effectively limit the growth rates along [111] and direct the synthesis of (111) enclosed nanotetrahedra. Mechanistic studies on the origin of the peptide recognition toward Pt(111) found that the phenyl ring within residue phenylalanine (F) is the effective motif to create binding contrast for the recognition process.[18] The derived principle has been further employed to the design of small organic molecules to achieve preferential binding to the (111) facets of both Pt and rhodium (Rh). Obviously, the phenyl ring plays a predominant role in guiding the molecular recognition and binding selectivity to (111) surfaces, suggesting a potential ground to explore the mechanisms contributing to the molecular facet-selective adsorption through the design of organic molecules to control the organic−inorganic interfacial reactions. Phenyl ring (or phenyl group) is derived from benzene and belongs to the chemical family of aromatic molecules. The interaction between aromatic molecules and various metal surfaces has been well studied in surface science, albeit in an environment different from practical syntheses, rendering an accessible library of references to facilitate the understanding of the molecular selective adsorption in colloidal nanocrystals.[19−22] Moreover, the variant substituent effect on aromatic molecules can be used to strategically tune their electronic properties and molecular structures, which are

Received: June 17, 2013
Published: September 19, 2013

   dx.doi.org/10.1021/ja406018u | J. Am. Chem. Soc. 2013, 135, 15489−15500

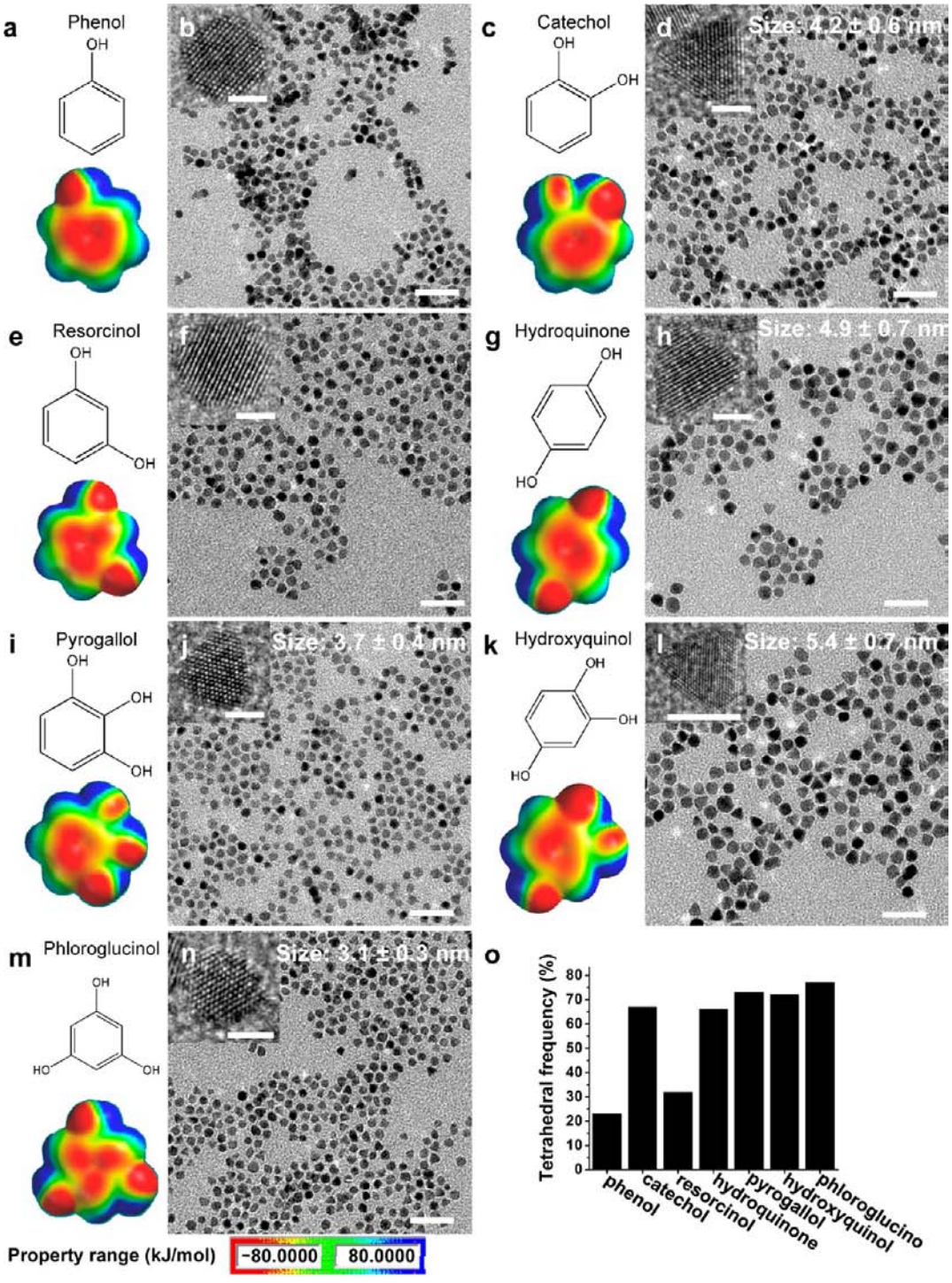

Figure 1. Pt nanocrystals controlled with a variety of phenolic molecules (hydroxyl group as substituent). (a,c,e,g,i,k,m) Molecular structures and electrostatic potential surfaces of (a) phenol, (c) catechol, (e) resorcinol, (g) hydroquinone, (i) pyrogallol, (k) hydroxyquinol, and (m) phloroglucinol. (b,d,f,h,j,l,n) Corresponding TEM images of the obtained Pt nanocrystals by phenolics and HRTEM images (in inset) of representative Pt cuboctahedra and tetrahedra in the syntheses. (o) Tetrahedral frequencies of Pt nanocrystals synthesized by different phenolics. Scale bars: 20 nm in (b,d,f,h,j,l,n); 2 nm in inset of (b,d,f,h,j,n); 5 nm in inset of (l). Electrostatic potential: [−80 kJ mol^{-1} (red) to +80 kJ mol^{-1} (blue)].

considered important parameters in determining the molecular binding configuration and strength.[23,24]

Herein, we present systematic studies on facet-selective adsorption of aromatic molecules on noble metal crystals. We demonstrate that selective adsorption can be guided by molecular electrostatic potential surfaces through controlled nanocrystal syntheses and Raman spectroscopy studies of the corresponding organic−inorganic interfaces. The negative electrostatic potential on the ring system of the aromatic molecules has been demonstrated to be the prerequisite to determine their binding selectivity to Pt(111) facets. A number of aromatic molecules substituted with variant functional

dx.doi.org/10.1021/ja406018u | J. Am. Chem. Soc. 2013, 135, 15489−15500

groups are compared in terms of their facet selectivity to Pt(111) facets, assessed by synthesizing shaped Pt nanotetrahedra. The geometric matching between molecular structures (functional groups acting as binding sites) and metal surface lattice is also found to be an important factor contributing to the facet specificity.[25,26] More importantly, we used Raman spectroscopy to probe the interactions between aromatic molecules and faceted Pt nanocrystals, providing direct evidence of the molecular binding mechanism and configurations on a particular crystal surface. This suggests a strategy to design Pt(100) facet-specific surfactants. In particular, we demonstrate that the organic molecules with both neutral to positive electrostatic potential on the ring and with geometric matching to Pt(100) lattice show Pt(100) facet specificity and can be used to synthesize Pt nanocubes. In addition to Pt, we further rationally design and identify Pd(111) and Pd(100) facet-specific surfactants and prove their selective binding through their effectiveness in guiding the syntheses of Pd nano-octahedra and Pd nanocubes, respectively. These results demonstrate the general applicability of the design guidelines discovered in this work. Therefore, the system of aromatic molecules and noble metal crystal facets provides a suitable platform to achieve better understanding of the organic−inorganic interfaces in colloidal nanocrystals, which significantly enriches our knowledge in their synthesis strategy and related applications.

EXPERIMENTAL SECTION

Chemicals. Chloroplatinic acid hydrate ($H_2Pt(IV)Cl_6{\cdot}xH_2O$, 99.9% trace metals basis), sodium tetrachloropalladate (II) (98%), sodium borohydide ($NaBH_4$, granular 99+%), L-ascorbic acid (99+), phenol (99+%), catechol (99+%), resorcinol (99+), hydroquinone (99+), pyrogallol (99+%), hydroxyquinol (99%), phloroglucinol (99+%), *p*-nitrophenol (99+%), gallic acid (98+%), *p*-aminophenol (98+%), syringol (99%), *p*-quinone (98+%), squaric acid (99%), and terephthalic acid (98%) were purchased from Sigma-Aldrich. Hydrochloric acid (37.2%) and *N*,*N*-dimethylformamide (DMF) were purchased from Fisher Scientific. All chemicals were used as received without further purification.

Synthesis of Pt nanocrystals. All regents used here are dissolved in water before use. 1 mM H_2PtCl_6 and 15 μg/mL of aromatic molecules (60 μg/mL for syringol) were premixed in a vial, and $NaBH_4$ aqueous solution with a final concentration of 1 mM (0.5 mM for phloroglucinol and gallic acid-controlled synthesis) was injected in one shot. TEM samples were prepared after 30 min of reaction. The total volume of all reaction solutions is 5 mL. The concentrations indicated are all final concentration. In the reactions to generate Pt nanocubes with ascorbic acid and *p*- nitrophenol, 1 mM of H_2PtCl_6 mixed with 0.5 mM of ascorbic acid and 12 μg/mL of aromatic molecules were injected with 2 mM $NaBH_4$, reacting for 1 h. In *p*-quinone-controlled synthesis of Pt nanocubes, 50 μL of 50 mM $NaBH_4$ was injected into 1 mM of H_2PtCl_6, after 30 s, 20 μL of 2 mg/mL of *p*-quinone (final concentration 8 μg/mL) was introduced; the total reaction time is 1 h. In squaric acid-controlled reaction, 1 mM $NaBH_4$ was injected into 1 mM of H_2PtCl_6 mixed with 0.5 mM of ascorbic acid and 8 μg/mL of squaric acid, reacting for 1 h. All reactions were conducted at ambient environment with stirring.

Synthesis of Pd nanocrystals. 3.5 mL DMF was first mixed with 0.375 mL water, 500 μL of 50 mM ascorbic acid in aqueous solution, and 3 mg of hydroquinone (for Pd octahedra) or 12 mg of terephthalic acid (for Pd cubes). The mixed solution was heated at 80 °C for 5 min and followed by an injection of 625 μL of 20 mM Na_2PdCl_4 aqueous solution. Transmission electron microscopy (TEM) samples of colloidal crystals were collected after one hour of reaction.

Characterization. The morphologies of the synthesized nanocrystals were imaged by a FEI CM 120 TEM operated at 120 kV and by a FEI TITAN high-resolution TEM (HRTEM) at 300 kV, respectively. All TEM samples for imaging were prepared by pipetting the solution onto carbon-coated copper grids. TEM samples were dried in atmosphere before images were taken. The Raman spectra were measured on a Renishaw inVia spectrometer system equipped with an argon ion laser, 50 mW at 514 nm, air cooled as excitation source. The laser spot size is around 1 μm. The spectral resolution was 4 cm^{-1} at the excitation wavelength. Typically, aromatic molecule-controlled nanocrystals were washed with water for two times by centrifuge (14 000 rpm, 30 min per cycle) to remove excessive reagents. The collected nanocrystals were incubated in 1 mg/mL of aromatic molecules in aqueous solution for 30 min and followed by centrifuge to remove excessive aromatic molecules. The final products of aromatic molecules on Pt nanocrystals were redispersed in water and drop-cased on aluminum foil to form a thin film for Raman spectroscopy. In particular, in order to characterize the adsorption behavior of *p*-nitrophenol on Pt(111) surface, Pt tetrahedra were synthesized with phloroglucinol and washed five times by centrifuge to remove phloroglucinol. The collected Pt tetrahedra were then incubated into *p*-nitrophenol, centrifuged and redispersed in water for drop-casting into film.

Computation. Electrostatic potential surfaces of organic molecules were computed by mapping electrostatic potential onto surfaces of molecular electron density (0.002 electrons/au^3) and color-coding, using Hartree−Fock and 6-31G* basis set to calculate equilibrium geometry at ground state by the program Spartan '06.[27] For all surfaces shown in this work, the potential energy values range from −80 kJ mol^{-1} (red) to 80 kJ mol^{-1} (blue). Red color represents a value equal to or greater than the maximum in negative potential, and blue corresponds to a value equal to or greater than the maximum in positive potential.

RESULTS AND DISCUSSION

We first studied the facet-selective adsorption of water-soluble phenolics containing a benzene ring with one to three hydroxyl groups at different sites. The binding selectivity of the phenolics to Pt(111) facets is reflected by the yield of Pt nanotetrahedra from the phenolics controlled syntheses.[18] The molecular structures and electrostatic potential surfaces of the studied phenolics are depicted in Figure 1a,c,e,g,i,k,m. The hydroxyl group with a π electron-donating property contributes to overall negative electrostatic potential on the aromatic ring. Most of the obtained Pt nanocrystals synthesized by phenol (with one hydroxyl group bonded to a benzene ring) and resorcinol (with two hydroxyl groups at the *meta* position), respectively, are cuboctahedra (Wulff polyhedrons) enclosed by a mix of (111) and (100) facets, suggesting they display no binding selectivity to Pt facets (Figure 1a,b,e,f and Table S1). Except for phenol and resorcinol, the aromatic molecules discussed in Figure 1 can synthesize well-dispersed Pt nanotetrahedra enclosed by (111) facets with high yield and different sizes as shown in Figure 1d,h,j,l,n,o, indicating their binding specificity to Pt(111) facets. The detailed shape distributions of the Pt nanocrystals in Figure 1 are listed in Table S1. Catechol with two hydroxyl groups at the *ortho* position can synthesize 67% of Pt tetrahedra with an average size of 4.2 ± 0.6 nm (Figure 1c,d,o). Hydroquinone with two hydroxyl groups at the *para* position yields 66% of Pt tetrahedra with an average size of 4.9 ± 0.7 nm (Figure 1g,h,o). Pyrogallol, hydroxyquinol, and phloroglucinol with three hydroxyl groups bonded to a benzene ring generate Pt nanocrystals with 73%, 72%, and 77% of tetrahedra and average sizes of 3.7 ± 0.4 nm, 5.4 ± 0.7 and 3.1 ± 0.3 nm, respectively (Figure 1i−o). The insets in Figure 1d,h,j,l,n represent the corresponding HRTEM images of different sized Pt nanotetrahedra mentioned above, showing a typical triangular projection of a tetrahedron. Figure S1a,b shows the HRTEM images of tetrahedra imaged along

dx.doi.org/10.1021/ja406018u | J. Am. Chem. Soc. 2013, 135, 15489−15500

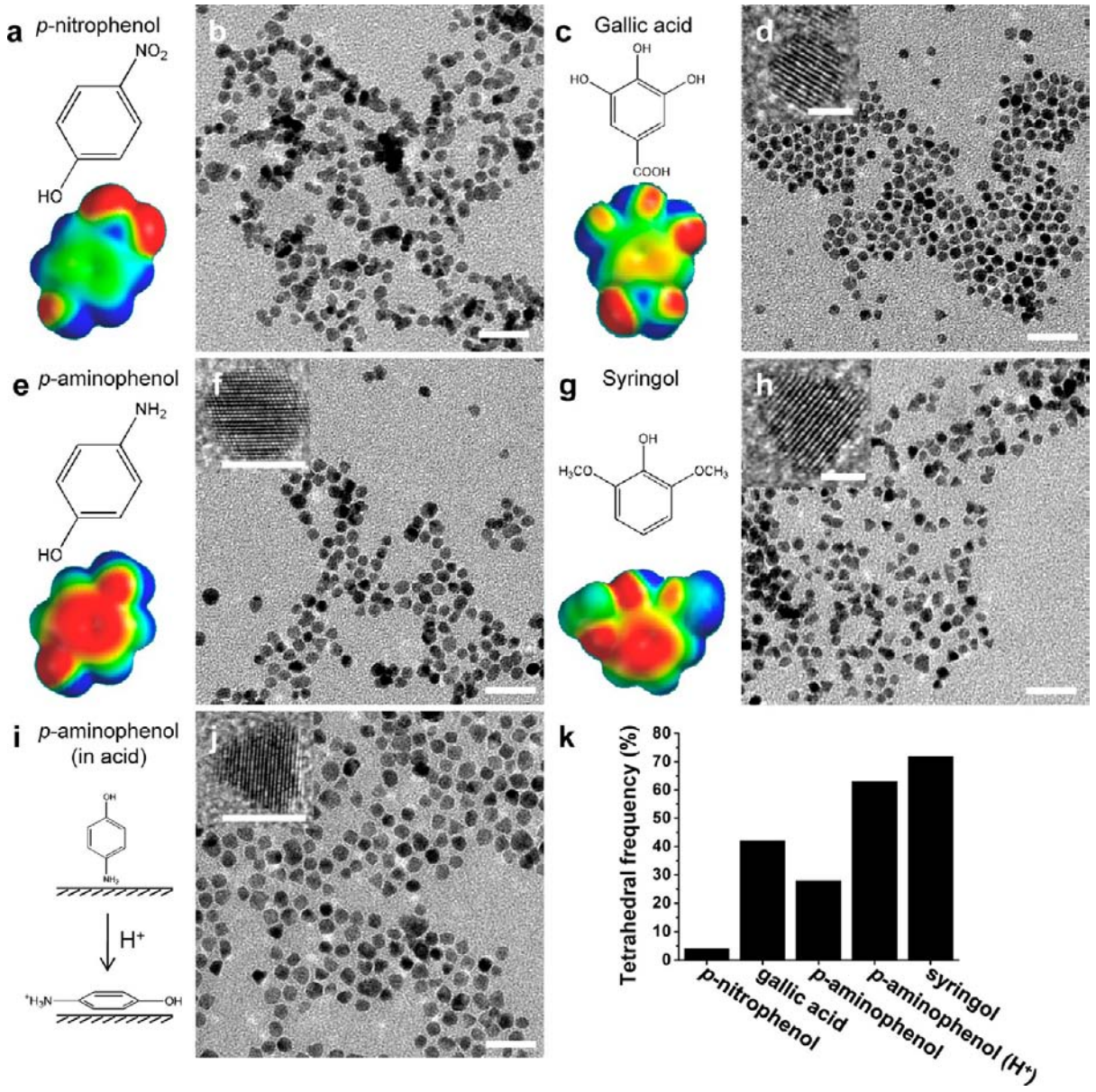

Figure 2. Pt nanocrystal controlled by phenolic molecules substituted with nitro, carboxyl, amine, and methoxy group, respectively. (a,c,e,g) Molecular structure and electrostatic potential surface of (a) *p*-nitrophenol, (c) gallic acid, (e) *p*-aminophenol, and (g) syringol; (b,d,f,h) corresponding TEM images of the obtained Pt nanocrystals. (i) Schematic illustration of switching the adsorption behavior of *p*-aminophenol by inactivating amine group in acid. (j) TEM image of Pt nanocrystals controlled by *p*-aminophenol in acidic solution (pH 4). Insets in (d,f,h,j) are the corresponding HRTEM images of the representative Pt cuboctahedra and tetrahedra. (k) Tetrahedral frequencies of Pt nanocrystals controlled with different aromatic molecules. Scale bars: 20 nm in (b,d,f,h,j); 2 nm in insets of (d,h); 5 nm in insets of (f,j). Electrostatic potential: [−80 kJ mol^{-1} (red) to +80 kJ mol^{-1} (blue)].

[110] and [112] directions, respectively, confirming that the triangular and diamond-like shapes observed in TEM images are tetrahedra. In contrast, Pt cuboctahedron is spherical (insets in Figures 1b,f and S1c). The TEM images of Pt nanocrystals obtained from the syntheses as a function of the concentration of phlorogulcinol indicate there is an optimal phloroglucinol concentration for the highest yield of tetrahedra with a satisfactory quality (Figure S2). Below the optimal phloroglucinol concentration there are not enough surfactant molecules to stabilize all (111) facets on the nanocrystal surface, while above that excessive surfactants may start to bind on nonspecific facets, both leading to less developed shapes. The control experiment in the absence of surfactant led to aggregated nanocrystals without well-defined shape, suggesting the exclusive effect of the aromatic molecules on shaping nanocrystals (Figure S2a). These observations are consistent with our previous study on Pt(111) facet-specific peptide.[17] With the exception of resorcinol, the yield of Pt nanotetrahedra increases with the number of hydroxyl groups on the benzene ring, indicating the interaction between the aromatic molecules and Pt(111) surface is enhanced by hydroxyl substitutions (Figure 1o). We believe that the position and the number of hydroxyl substitutions on an aromatic ring could affect the whole molecule's binding strength to Pt(111) and consequently the yield of tetrahedral Pt nanocrystals. Moreover, using different synthetic conditions with different Pt precursors, we can synthesize larger nanocrystals (>6 nm) with the aromatic molecules and observe similar phenomena in terms of their

dx.doi.org/10.1021/ja406018u | J. Am. Chem. Soc. 2013, 135, 15489−15500

Pt(111) facet binding selectivity, further confirming their role in nanocrystal synthesis (Figures S3 and S4).

It is generally accepted that benzene adsorbs on Pt(111) at the bridge (30) position, wherein C p_z orbitals overlapping with the metal d_{z^2} and d_{yz} orbitals lead to the formation of Pt−C bonds.[19,20] This interaction is explained by electron donation from the molecular π orbitals of benzene to the surface d-band of Pt and back donation from the surface to the molecular π^* orbitals of benzene.[21,22] In addition, the strength of the interaction depends on the ability of the metal to act as an acceptor, which in turn depends on the work function of the metal.[28] Phenolics, which have higher highest occupied molecular orbital (ε_{HOMO}) levels than benzene, can act as electron donors.[29] In comparison with Pt(100), Pt(111) has a higher work function and therefore is a more effective acceptor, which facilitates better electron donation from the aromatic molecule, leading to a stronger interaction between the surface d states and the delocalized π electrons of phenolics.[30,31] These effects contribute to the binding selectivity of phenolics to Pt(111) facets and explain the production of Pt nanotetrahedra. Hydroxyl substitution can enhance the π donating tendency of the host aromatic ring, further increasing the interaction strength between the phenolics and Pt(111) facets. This is supported by the increasing yield of Pt tetrahedra in the following order: phenol (1-OH) < catechol and hydroquinone (2-OH) < pyrogallol, phloroglucinol and hydroxyquinol (3-OH). Similar trend of stronger organic−inorganic interactions upon increasing the number of hydroxyl substitutions in phenolics has been reported previously.[32] The position of the hydroxyl substituent can change the π electron distribution in the ring region and hence may also play a role in the facet selectivity. Comparing the electrostatic potential surfaces of catechol, resorcinol and hydroquinone (Figure 1c,e,g), the red region in the ring system of catechol and hydroquinone is symmetric, while that of resorcinol is relatively asymmetric (Figure S5a).This difference may alter the preferential adsorption geometry of benzene ring on Pt(111) surface (e.g., from bridge position to three-fold hollow), which can decrease the possible molecular binding sites (or the associated Pt atoms) for resorcinol binding on (111) (Figure S5b). This change can eventually lead to the loss of molecular binding preference on Pt(111), accounting for the low yield of tetrahedra synthesized by resorcinol. In addition to benzene ring, active functional groups, such as hydroxyl and amine groups, can act as binding sites on metal surfaces, pointing to the importance of the geometric relationship between the positions of hydroxyl groups and lattice of Pt(111).[33,34] By locating the benzene ring on the bridge (30) position (considered as the most stable configuration),[19,20] we geometrically match hydroxyl groups of hydroquinone, pyrogallol, and phloroglucinol to Pt(111) surface atoms (Table S2). Significantly, the hydroxyl groups can be well located on the preferential binding sites (top or bridge) on the Pt(111) surface with little lattice mismatch. Therefore, increasing number of hydroxyl groups can contribute to the increased interaction between phenolics and Pt(111) surface, again confirming our experimental results. To summarize, phenolics with negative electrostatic potential on the ring system display binding selectivity to Pt(111) facets, while the position and number of hydroxyl substituents can alter their facet selectivity and binding strength.

It is known that the phenolics with hydroxyl substituent can be used as reducing agents, and their redox potential related to the substituent position decreases in the order of *meta-*, *ortho-*, and *para-* substitution.[35,36] We found the reducing power of phenolics used here increases in the order of phloroglucinol, pyrogallol, catechol, hydroquinon and hydroxyquinol, which agrees with the increase in the size of Pt tetrahedra controlled by them (Figure 1d,h,j,l,n). It is possible that the molecules adsorbed on the metal surface may help reduce Pt ions locally and grow larger nanocrystals. These locally oxidized molecules may be in the form of radical and lose binding effect but can be instantly recovered by $NaBH_4$ once they dissociate from the Pt surface. Phenolics solely cannot reduce Pt(IV) ions to generate Pt nanocrystals without introducing $NaBH_4$ in the reactions. More investigation is needed to elucidate the size variation of the Pt nanocrystals synthesized by different aromatic molecules. Nevertheless, we believe phenolics in the vincinity of the Pt surfaces stay in the reduced form due to the reducing environment, supported by the UV−vis spectra of hydroquinone, *p*-quinone, and hydroquinone-Pt nanocrystals solution (Figure S6). It is showed that hydroquinone did not oxidize to *p*-quinone (appearance of absorption at 244 cm) in our Pt synthesis reaction after 30 min of reaction time.[37]

We continue to study the facet selective adsorption of aromatic molecules substituted with other functional groups, such as nitro and amine groups. These groups will alter the electrostatic potential on the benzene ring and interact with Pt surface differently. As shown in Figure 2a,c, *p*-nitrophenol and gallic acid substituted with π electron-withdrawing nitro and carboxyl group, respectively, show less negative to neutral electrostatic potential on the aromatic ring relative to those shown in Figure 1. We observed that *p*-nitrophenol showing almost neutral electrostatic potential on the ring (ranging from −10 to 0 kJ mol^{-1}) generates aggregated Pt nanocrystals without well-defined shapes (Figure 2a,b). However, gallic acid showing negative electrostatic potential on the ring (ranging from −50 to −10 kJ mol^{-1}) yields Pt nanocrystals with 42% of tetrahedra and 56% of cuboctahedra (Figure 2c,d,k and Table S1). Obviously, as the electrostatic potential on the ring changes from neutral (*p*-nitrophenol) to negative (gallic acid), the yield of Pt tetrahedra increases accordingly from 4% to 42%, demonstrating that the molecular electrostatic potential surfaces can be used to guide the molecular binding selectivity to Pt(111) facets (Figure 2a,c,k). Nevertheless, in comparison with Figure 1, the aromatic molecules substituted with π electron-withdrawing group and showing less negative to neutral electrostatic potential on the ring produce a relatively low yield of Pt tetrahedra, indicating less Pt(111) facet preference. Amine and methoxyl groups known as electron donors can induce negative electrostatic potential on the ring of the aromatic molecules substituted with them. According to our hypothesis, *p*-aminophenol and syringol shown in Figure 2e,g are promising to show binding selectivity to Pt(111) facet and achieve the synthesis of Pt tetrahedra. However, it is worth noting that the different function groups (amine, methoxyl, and hydroxyl) on the benzene ring can alter the molecular adsorption behavior on Pt surface. We demonstrate that the interactions between the amine group in *p*-aminophenol and the Pt surface are stronger, which tend to erect the whole molecule off the surface.[38] This results in the loss of binding selectivity to Pt(111) facet and leads to a low yield of Pt tetrahedra (28%), as shown in Figure 2f,k.[34,39] By tuning the pH of the reaction solution from 6 to 4, a tetrahedral yield of 63% is obtained (Figure 2f,j,k). In the acidic solution the amine group of *p*-aminophenol is more protonated, weakening its

dx.doi.org/10.1021/ja406018u | J. Am. Chem. Soc. 2013, 135, 15489−15500

interaction with the Pt surface.[34] Under this condition, the aromatic ring with negative electrostatic potential predominantly contributes to the surface binding and selective adsorption on Pt(111) surface (Figure 2i).[34] The change of adsorption configuration is further proven by Raman spectroscopy (Figure 4). While substituted with two methoxyl groups and one hydroxyl group, syringol is like pyrogallol in terms of the electrostatic potential on the ring and the position of the three π electron donors (Figure 2g), indicating the two aromatic molecules may share similar facet binding selectivity to Pt(111).[36] The methoxyl group in syringol consisting of a methyl group bound to oxygen is bulkier than the hydroxyl group, so its steric effect on binding to Pt(111) is expected (Figure 2g).[34] Although the steric effect of methoxyl group can weaken the expected binding strength of syringol to Pt(111), a comparable yield of Pt nanotetrahedra (72%) can be achieved with a higher concentration of syringol 60 μg/mL (pyrogallol: 15 μg/mL) (Figure 2h,k and Table S1). This suggests that syringol has Pt(111) facet binding specificity as guided by the electrostatic potential surface. Taken together, the negative electrostatic potential on the ring acts as the prerequisite to determine the Pt(111) facet specificity of aromatic molecules, although the different substituent-metal surface interaction may influence the molecular binding behavior. The pH of all reactions, 5−6, was lower than the pK_a of the aromatic molecules, indicating the molecules used in reactions might not be highly charged and primarily stay in their neutral forms (Table S1).

The adsorption behavior of benzene and substituted benzene on different metal surfaces has been extensively explored through surface characterization techniques.[28,39,40] Those studies may not apply directly to our systems but provide useful information that can be used to interpret our observations. Here, we used Raman spectroscopy to characterize the adsorption of aromatic molecules on different Pt surfaces. The obtained results can not only provide direct evidence of the molecular binding configuration and mechanism but also aid to discover more facet-specific surfactants. As shown in Figure 3, the Raman spectra of free hydroquinone molecules and hydroquinone on Pt nanotetrahedra [hydroquinone-Pt(111)] differ noticeably. The assignment of the peaks observed in the Raman spectra to the vibrational modes of hydroquinone is shown in Table 1.[41] The C−H stretch

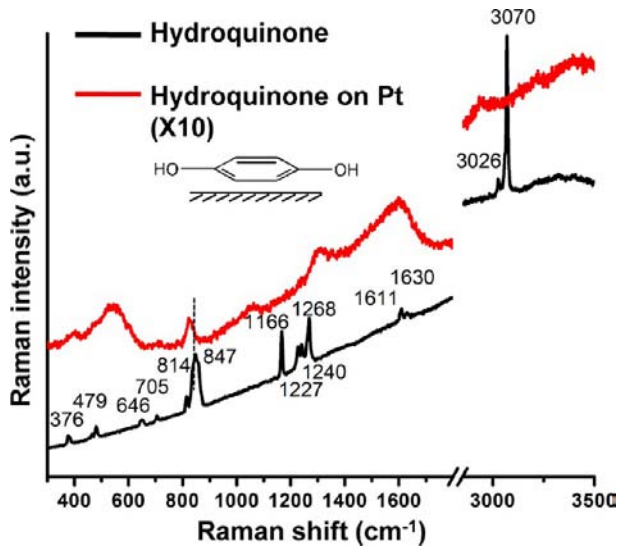

Figure 3. Raman spectra of free hydroquinone (black line) and hydroquinone on Pt tetrahedra [(111) faceted] (red line).

Table 1. Assignment of the Vibrational Modes of Raman Peaks for Hydroquinone

Free hydroquinone	Hydroquinone on Pt(111)	Assignment
3070, 3026	2935	C-H stretch
1630, 1611	1600	C-C ring stretch
1268	1313	C-O stretch
1240, 1227		O-H in plane bend
1166	1063	C-C-H in plane bend
847	823	C-C ring stretch
814	781	C-H out of plane deformation
705		Ring torsion
646		C-C-C bend
	545	Pt-O/ Pt-C
479	466	C-C-C bend
376	404	C-O out of plane deformation

mode of hydroquinone at 3070 cm^{-1} (with a shoulder at 3026 cm^{-1}) shows a red shift of 91−135 cm^{-1} after binding to Pt(111) surface (Figure 3 and Table 1). C−C ring stretch modes at 1611 cm^{-1} (with a shoulder at 1630 cm^{-1}) and 847 cm^{-1} also have an obvious red shift of 30−11 and 24 cm^{-1}, respectively, upon adsorption (Figure 3 and Table 1). These two significant red shifts are similar to the observations for parallel-chemisorbed benzene on Pt(111) surface, confirming that the hydroquinone interacts with the Pt(111) surface via the π electron of the benzene ring with a flat orientation to the surface.[40,42,43] It is worth noting that the peak at 1268 cm^{-1} attributed to the C−O stretch mode of hydroquinone shifts to 1313 cm^{-1} upon adsorption, indicating that the hydroxyl groups interact with the Pt metal surface (Figure 3 and Table 1).[40,42] In addition, the disappearance of the O−H in-plane-bending peaks at 1240 and 1227 cm^{-1} as well as the peak found at 545 cm^{-1} attributed to the Pt−O bond in the spectrum of hydroquinone-Pt(111) strongly support our suggestion that hydroxyl groups contribute to the binding of hydroquinone on Pt(111) (Figure 3 and Table 1).[39,40] The red shift and intensive enhancement of the C−C ring stretch might infer a selective enhancement resulting from the charge-transfer enhanced effect, surface enhanced Raman scattering (SERS) (Figure 3).[42,44] Therefore, the configuration of hydroquinone on Pt(111) as we proposed in Table S2 is evident by the adsorption behavior observed from Raman spectra, indicating that hydroquinone interacts with Pt(111) with a flat aromatic ring on the surface and bonds via hydroxyl groups.

Figure 4 shows the Raman spectra of free *p*-aminophenol molecules and *p*-aminophenol on the as-synthesized Pt nanocrystals; the assignment of peaks is given in Table 2.[45] An intensive peak at 3071 cm^{-1} attributed to C−H stretch mode of *p*-aminophenol shows a slight red shift to 3077 cm^{-1} upon adsorption as well as the C−H in-plane-bending vibration, suggesting the interaction between the aromatic ring and Pt surface is weak (Figure 4 and Table 2). Another

dx.doi.org/10.1021/ja406018u | J. Am. Chem. Soc. 2013, 135, 15489−15500

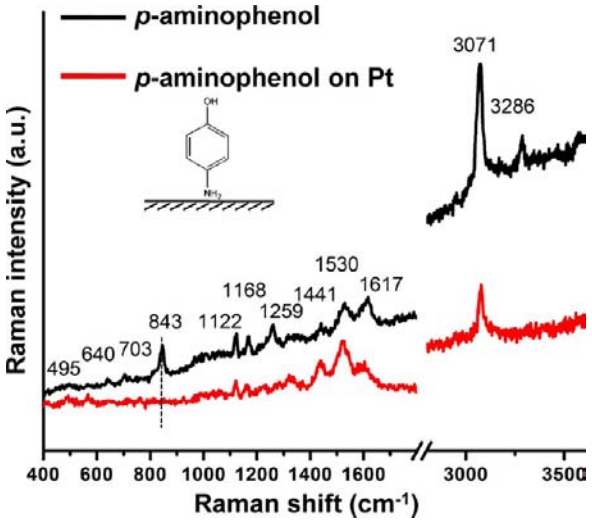

Figure 4. Raman spectra of free *p*-aminophenol (black line) and *p*-aminophenol on Pt nanocrystals (red line).

Table 2. Assignment of the Vibrational Modes of Raman Peaks for *p*-Aminophenol

Free *p*-aminophenol	*p*-aminophenol on Pt nanocrystals	Assignment
3286		O-H stretch
3071	3077	C-H stretch
1617	1603	C-C ring stretch
1530	1519	
1441	1440	
1259	1284	
1317	1322	
1168	1164	C-H in plane bend
1122	1120	
843		C-C ring stretch
703	761	NH_2 wag
640		C-C out of plane ring deformation
	566	Pt-O/ Pt-N
495	490	C-NH_2 out of plane bend

significant feature of the Raman spectra is the peak at 843 cm^{-1} attributed to the C−C ring stretch mode of *p*-aminophenol, which disappears upon adsorption, suggesting a vertical orientation of the ring to Pt surface (Figure 4 and Table 2).[43] As we discussed above, the active amine group interacts with the Pt surface stronger than the phenyl ring and hydroxyl group, leading to *p*-aminophenol binding on the Pt surface via primary interaction through the amine group. We confirm this binding configuration on the observation of the large shift of NH_2 wag mode from 703 to 761 cm^{-1} (Figure 4 and Table 2). However, *p*-aminophenol binding on the Pt surface though the aromatic ring still contributes to part of whole binding behavior since relative shifts of the peaks from the C−C ring stretch modes ranging from 1617 to 1317 cm^{-1} upon adsorption are observed (Figure 4 and Table 2). Overall, a lack of strong interaction between the aromatic ring and Pt surface results in the loss of binding selectivity of *p*-aminophenol to the Pt(111) surface, consequently contributing to the observed low yield (28%) of Pt tetrahedra controlled by *p*-aminophenol (Figure 2e,k) at pH = 6.

To enhance crystal growth, we introduced ascorbic acid as a secondary and mild reducing agent like our previous study, in which ascorbic acid can continue reduce the residual Pt ion for preferential atom addition controlled by surfactants.[17] Figure S7 and Table S3 show Pt nanotetrahedra remain predominant in the obtained Pt nanocrystals synthesized by hydroquinone and phloroglucinol in the reactions with ascorbic acid, respectively. Similar to the results shown in Figures 1 and 2, resorcinol, *p*-aminophenol, and gallic acid show much weaker binding selectivity to Pt(111) facets produce low yield of Pt tetrahedra (Figure S7 and Table S3), indicating ascorbic acid barely interferes their binding behavior. Surprisingly, through enhancing the crystal growth, Pt nanocrystals controlled with *p*-nitrophenol can grow 66% of cubes enclosed by (100) facets with an average size of 7.3 ± 0.9 nm, suggesting *p*-nitrophenol, to some extent, has binding selectivity to Pt(100) facets (Figure 5a,b). Compared to the electrostatic potential of the phenolics

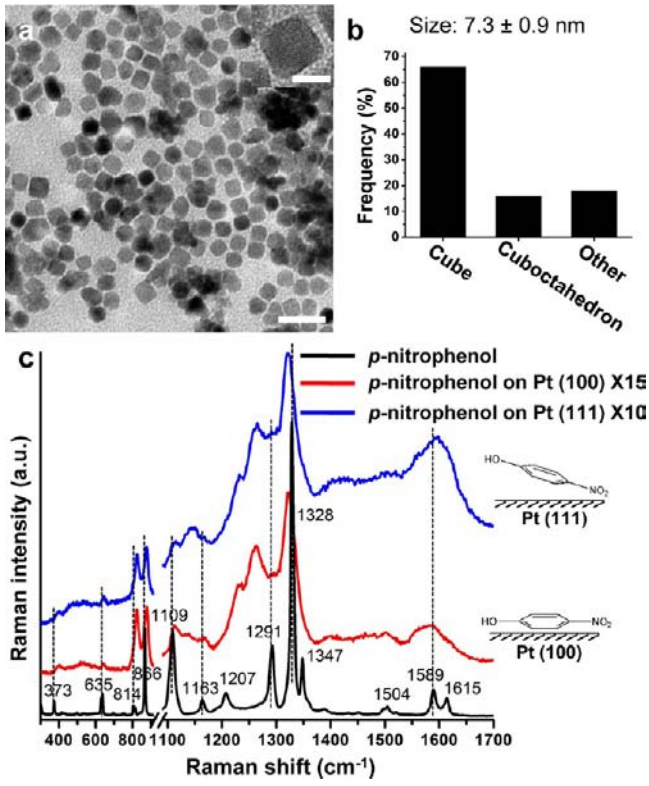

Figure 5. (a) TEM image of *p*-nitrophenol control synthesis of Pt nanocubes. (b) The corresponding size and shape distribution of (a). (c) Raman spectra of free *p*-nitrophenol (dark line), and *p*-nitrophenol on Pt nanocubes [(100) faceted] (red line) and Pt nanotetrahedra [(111) faceted] (blue line), respectively. Scale bars: 20 nm in (a); 5 nm in inset of (a).

in Figure 1 and Figure 2, *p*-nitrophenol has almost neutral potential on the ring, which could be an important guidance to select Pt(100) facet-specific molecules. To study the facet adsorption behavior of *p*-nitrophenol on Pt, we used Raman spectroscopy to characterize free *p*-nitrophenol molecules, *p*-nitrophenol on Pt nanotetrahedra [(111) faceted], and *p*-nitrophenol on Pt nanocubes [(100) faceted], respectively, as shown in Figure 5c. The three spectra show similar characteristic peaks, while some of them vary obviously in frequency,

dx.doi.org/10.1021/ja406018u | J. Am. Chem. Soc. 2013, 135, 15489−15500

indicating they display different adsorption behavior on Pt(111) and Pt(100) surface. First, the peak at 1589 cm^{-1} attributing to C−C ring stretching mode has a blue shift to 1597 cm^{-1} upon adsorption on Pt(111) while shows nearly no shift on Pt(100) (Figure 5c and Table 3).[46] It is reported that tilted chemisorbed benzene interacting with metal surface may show a small blue shift in the ring breath vibration, suggesting *p*-nitrophenol might have a tilted ring orientation to Pt(111).[43] Second, the NO_2 relevant vibration modes including symmetric NO_2 stretching at 1328 cm^{-1} and NO_2 bending at 866 and 814 cm^{-1} show more significant shift upon adsorption on Pt(111) than on Pt(100), indicating nitro group interacts more strongly with Pt(111) (Figure 5c and Table 3).[42] Moreover, the significant red shift of C−O stretching mode at 1291 cm^{-1}, and the appearance of a shoulder peak [i.e., 1233 cm^{-1} for Pt(111) and 1236 cm^{-1} for Pt(100)] are observed, indicating the interaction between hydroxyl group and Pt surfaces (Figure 5c and Table 3).[44] These results conclude that *p*-nitrophenol adopts a tilted configuration on Pt(111) through the end group of either OH or NO_2. It also confirms the lack of direct interaction between aromatic ring and Pt(111), leading to the loss of the molecular binding selectivity to Pt(111). In the case of *p*-nitrophenol on Pt(100), in addition to C−C ring stretching mode, the other ring associated characteristic peaks (i.e., C−H in plane bending at 1504 and 1109 cm^{-1}, and C−C−C bending at 635 cm^{-1}) show small or almost no shift, indicating the lack of interaction between the ring and the (100) metal surface. We suggest that both groups (OH and NO_2) interact with Pt(100) at the same time by observing the relative shift of their vibration modes (e.g., NO_2 and C−O stretching and NO_2 bending). We believe *p*-nitrophenol's interaction with Pt(100) surface is not through the ring since it is π electron deficient relative to those Pt(111) facet-specific molecules, and the corresponding Raman spectrum showed a similar ring vibration frequency as that found in free *p*-

Table 3. Assignment of the Vibrational Modes of Raman Peaks for *p*-Nitrophenol

Free *p*-nitrophenol	*p*-nitrohpenol on Pt(100)	*p*-nitrohpenol on Pt(111)	Assignment
1615			C-C ring stretch
1589	1588	1597	
1504	1500		C-H in plane bend
1347			C-C ring stretch
1328	1324	1320	Sym NO_2 stretch
1291	1262	1264	O-C stretch
	1236	1233	
1207			C-H in plane bend
1163	1167	1150	C-O-H bend
1109	1112	1115	C-H in plane bend
866	877	878	NO_2 bend
814	823	825	
635	636	643	C-C-C bend
	517	532	Pt-O / Pt-N
373	400	401	O-C torsion

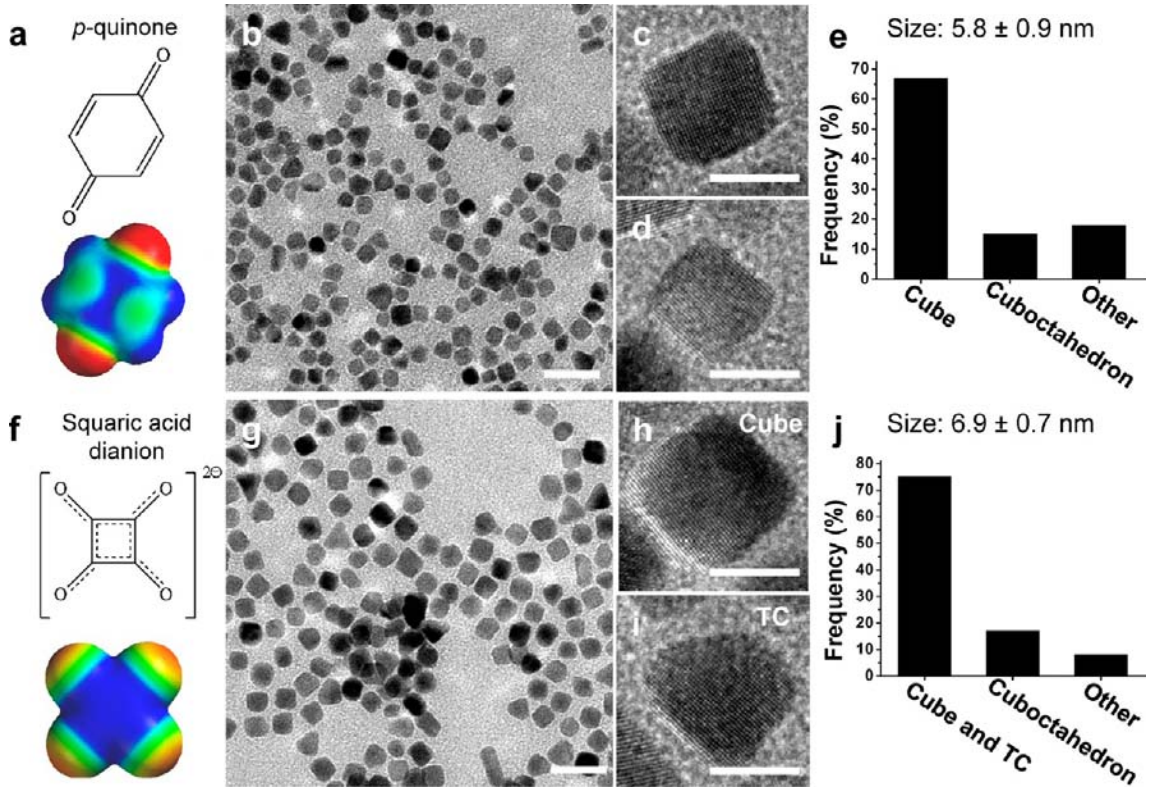

Figure 6. Pt nanocubes controlled by molecules with a positive electrostatic potential surface. (a,f) Molecular structure and electrostatic potential surface of (a) *p*-quinone and (f) dianion of squaric acid. (b,g) TEM images of the obtained Pt nanocrystals. (c,d) and (h,i) are HRTEM images of Pt nanocrystals observed in (b) and (g), respectively. (e) and (j) are the corresponding size and shape distributions of nanocrystals in (b) and (g), respectively. Scale bars: 20 nm in (b,g); 5 nm in (c,d,h,i). TC: truncated cube. Electrostatic potential: [−80 kJ mol^{-1} (red) to +80 kJ mol^{-1} (blue)].

dx.doi.org/10.1021/ja406018u | J. Am. Chem. Soc. 2013, 135, 15489−15500

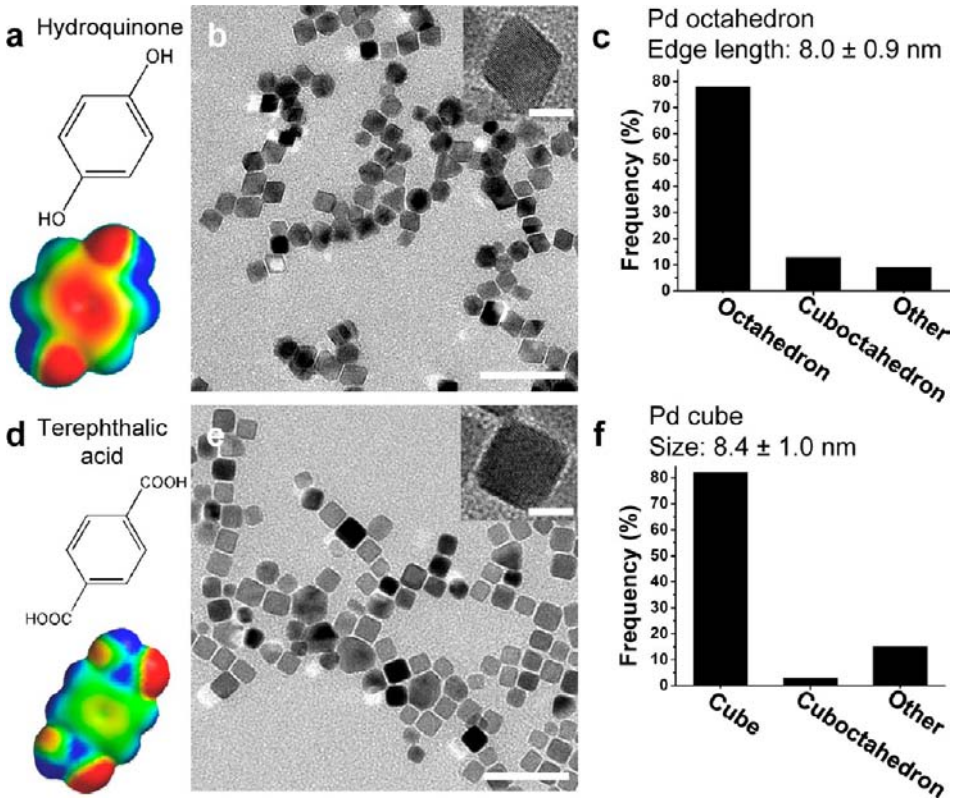

Figure 7. Pd nano-octahedra and nanocubes synthesized by hydroquinone and terephthalic acid, respectively. (a) and (d) are molecular structure and electrostatic potential surface of hydroquinone and terephthalic acid, respectively. (b) TEM image of Pd nanocrystals controlled by hydroquinone; inset: HRTEM image of a Pd octahedron. (e) TEM image of Pd nanocrystals controlled by terephthalic acid; inset: HRTEM image of a Pd cube. (c and f) Shape distributions of hydroquinone (c) and terephthalic acid (f) controlled synthesis of Pd nanocrystals. Scale bars: 40 nm in (b, e); 5 nm in insets of (b, e). Electrostatic potential: [−80 kJ mol^{-1} (red) to +80 kJ mol^{-1} (blue)].

nitrophenol molecules. Therefore, the hydroxyl and nitro groups of *p*-nitrophenol might predominantly contribute to the Pt(100) binding specificity. By matching its molecular structure to Pt(100) lattice, we can well locate benzene ring at four-fold hollow site, two oxygens of nitro group on top of Pt atoms and hydroxyl group on hollow site (see Table S4) with little lattice mismatch. This suggests the geometric matching relationship between molecular binding sites, and Pt(100) lattice is important in determining (100) facet-specific surfactants.

Guided by the adsorption behavior of *p*-nitrophenol on Pt surfaces, we conclude the directions to select molecules with Pt(100) facet binding specificity. First, the molecule should have almost neutral electrostatic potential on its ring. Second, there is geometric matching relationship between the functional groups and Pt(100) lattice, which directly contributes to the binding. To further demonstrate the guidelines, we rationally select *p*-quinone and squaric acid as Pt(100) facet-specific surfactants to control Pt nanocubes synthesis. As shown in Figure 6a,f, both of *p*-quinone and squaric acid (in the form of dianion) have a blue region on their ring corresponding to positive electrostatic potential (+80 kJ mol^{-1}), indicating a more π electron-deficient ring than that of *p*-nitrophenol. Moreover, the oxygen of their carbonyl groups can well match the hollow site or top of Pt atoms on Pt(100) lattice by locating the rigid ring on the four-fold hollow position (considered as the most stable configuration) (Table S4). As expected, *p*-quinone and squaric acid can regulate 67% of Pt nanocubes with an average size of 5.8 ± 0.9 nm and 75% of Pt nanocubes with an average size of 6.9 ± 0.7 nm, respectively (Figure 6b,e,g,j), suggesting their binding selectivity to Pt(100) facets. For the *p*-quinone-controlled synthesis of Pt nanocubes, we reduced the concentration of $NaBH_4$ to 0.5 mM and introduced *p*-quinone into the reaction after 30 s of injecting $NaBH_4$. This method aims to minimize the interaction between $NaBH_4$ and *p*-quinone, which might change the binding effect of *p*-quinone on Pt(100).[47] Figure S8a−d shows the shape evolution of Pt nanocubes with time after introducing *p*-quinone. As time goes by, Pt nanocrystals grow and evolve to Pt nanocubes with the increased yield of Pt nanocubes from 15% to 67% (Figure S8). The corresponding HRTEM images in Figure 6c,d show a 7 and 5 nm Pt nanocube, respectively, confirming the obtained Pt nanocrystals in Figure 6b are shaped as cubes. The geometric model of cube, truncated cube, and cuboctahedron as well as their corresponding HRTEM images are given in Figure S9, indicating the cubic and spherical nanocrystals observed in the TEM image are cubes [enclosed by (100) facets] and cuboctahedra [enclosed by a mix of (100) and (111) facets], respectively. The control reaction without the separated addition of *p*-quinone and $NaBH_4$ shows the obtained Pt nanocrystals are not well-shaped (Figure S10a). Figure S10b shows the TEM image of Pt nancrystals with various shapes obtained from a blank control reaction (without *p*-quinone), suggesting the (100) binding effect of *p*-quinone on shaping Pt nanocubes. Squaric acid is known as a strong acid with pK_2 = 2.2, so it should appear in the form of dianion (all carbon atoms have sp^2 hybridization with symmetric C−C and C−O bonds) in the synthetic solution with pH = 4 (Figure 6f).[48] The obtained nanocrystals from the squaric acid-

dx.doi.org/10.1021/ja406018u | J. Am. Chem. Soc. 2013, 135, 15489−15500

controlled synthesis include cubes and some truncated cubes [predominately enclosed by (100) facets] as shown in Figure 6g−i. HRTEM images and their corresponding geometrical models of different projections of truncated cubes are shown in Figure S11, confirming the incomplete cubic projection found in TEM image are Pt nanocubes. To conclude, we successfully employ the discovered principles to rationally select Pt(100) facet-specific surfactants and demonstrate their effectiveness in controlled syntheses of Pt nanocubes through selectively binding on Pt(100).

Our discoveries from Pt system are transferable to another metal system, in particular, palladium (Pd). Since Pd and Pt share the same crystal structure (face-centered cubic) and a small lattice mismatch (0.77%), they have been used to synthesize bimetallic core−shell nanocrystals based on their favorable epitaxial relationship.[49] We can expect that the molecules showing geometric matching on Pt surfaces could perform similarly on Pd surfaces. On the other hand, work function of Pd is lower than of Pt, which should decrease the tendency of π electron donation from the ring system to Pd and lead to a weaker Pd-aromatic molecules interaction.[28] To establish a clear panel of these energy levels, we used DFT-PBE calculations to derive ε_{HOMO} of the organic molecules studied here and the work functions of Pt and Pd surfaces (see Table S5 for calculation results and details). By setting vacuum level as 0 and Fermi level (E_F) of metal as $-\phi$ (ϕ: work function of clean metal surface), the HOMO energy levels of molecules and work functions (or Fermi level) of different metal surfaces can be compared. To achieve charge-transfer interaction, ε_{HOMO} of aromatic molecules should be higher than E_F of the specific metal surface, which is evident for Pt(111) binding specific molecules (Table S5). Similarly, aromatic molecules with higher ε_{HOMO} than E_F of Pd(111) will more likely bind to it. As shown in Table S5, considering the tendency to induce charge transfer, phloroglucinol is excluded in binding to Pd(111), since its ε_{HOMO} is lower than E_F of Pd(111). Catechol and pyrogallol, with ε_{HOMO} close to E_F of Pd(111), are not effective, either. Syringol and *p*-aminophenol are also excluded because their functional groups might interact with Pd surfaces differently. Therefore, only hydroquinone and hydroxyquinol are potential candidates for selective binding on Pd(111) facets. As expected, hydroquinone (ε_{HOMO}: −5.34) was found to be able to yield 78% of Pd nano-octahedra [enclosed by Pd(111) facets] with average edge length of 8.0 ± 0.9 nm (Figure 7a−c), indicating its Pd(111) facet specificity [E_F of Pd(111): −5.59]. Additional HRTEM images of Pd octahedra recorded along different directions are shown in Figure S12. However, hydroxyquinol failed to control the formation of Pd octahedra (Figure S13a). We suspect that hydroxyquinol may get oxidized in the reaction (80 °C) and lose binding specificity to Pd(111), since it should be the most active among the discussed phenolics.[50] Blank reaction and the other control experiments with Pt(111) facet-specific molecules, such as phloroglucinol and catechol, cannot generate well-defined Pd nanocrystals (Figure S13b−d), suggesting the exclusive binding selectivity of hydroquinone to Pd(111) facet and the success of our selection approach. In addition, we select terephthalic acid with almost neutral electrostatic potential (ranging from −20 to 10 kJ mol^{-1}) on the center and with geometric matching to Pd(100) (Figure 7d and Table S6) to be a Pd(100) facet-specific surfactant. As expected terephthalic acid can control the synthesis of Pd nanocubes with a yield of 82% and an average size of 8.4 ± 1.0 nm (Figure 7e,f), confirming its Pd(100) facet specificity. Interestingly, terephthalic acid can also be used to synthesize Pt nanocubes, showing binding effect on Pt(100) facets (Figure S14). However, we observed Pt(100) binding molecules (e.g., *p*-quinone and squaric acid) are not effective in shaping Pd nanocubes (Figure S13e,f), indicating these molecules might show different binding effect on Pd. Two possible reasons may account for this difference between Pt and Pd system. First, the ring system of *p*-quinone and squaric acid is electron deficient (positive electrostatic potential), which can serve as acceptor and induce electron donation from metal to molecules.[26] This is more likely to happen in Pd system instead of Pt since the ionization potential of Pd is ∼1 eV less than that of Pt.[51] Thus, we suggest that the "positive" ring systems in *p*-quinone and squaric acid cannot interact effectively with Pt(100) and Pt(111), wherein the geometric matching of the functional groups dominates interfacial interactions and results in preferential binding toward Pt(100). However, the ring systems in both molecules are more likely to bind with both Pd(100) and Pd(111), leading to the loss of facet specificity on Pd surfaces. At the same time, the ring system in terephthalic acid is neutral, which is unlikely to interact with neither metal surfaces through charge transfer, leaving the geometric matching dominates the binding specificity on both Pt(100) and Pd(100). Second, comparing the molecular structures of *p*-quinone and squaric acid to that of terephthalic acid, apparently, terephthalic acid with a benzene ring and two carboxyl groups shows a larger footprint in binding on metal surfaces, i.e., interaction with more Pt or Pd surface atoms (Table S4 and S6). Thus, terephthalic acid is potentially a stronger binder on (100), accounting for its binding selectivity on both Pt and Pd (100) surface. The molecular selection approach based on electrostatic potential and geometric matching has been demonstrated effective in designing and identifying Pd(111) and Pd(100) facet-specific molecules, representing a step forward to generalize the binding mechanism of organic surfactants on inorganic materials.

■ CONCLUSIONS

We have successfully formulated rational approaches to designing organic molecules with predictable binding selectivity to metal surfaces, guided by their molecular electrostatic potential surface, along with soft-epitaxial matching.[18,52] The negative electrostatic potential on the ring system of aromatic molecules is the prerequisite to determine the binding selectivity to Pt(111) facets. The electrostatic potential can be tuned by the number, position and electron affinity of the substituents on the ring, suggesting a controllable method to modulate the facet selectivity as well as the organic−inorganic interface. The geometric matching relationship between the structures of aromatic molecules and the Pt(111) surface also contributes to the binding mechanisms. Based on our discoveries, several aromatic molecules showing Pt(111) facet binding specificity are identified and applied to generate Pt nanotetrahedra. Through Raman characterization, we can infer the molecular binding configurations on the metal surfaces. It is evident that hydroquinone with Pt(111) facet binding specificity adsorbs parallel to Pt(111) surface via aromatic ring and hydroxyl groups. However, *p*-aminophenol interacts with the Pt surfaces through the amine group, losing the binding selectivity to Pt(111) facets. On the other hand, we discovered that organic molecules, such as *p*-nitrophenol, *p*-quinone, and squaric acid with almost neutral to positive electrostatic potential on the aromatic ring, can synthesize Pt

nanocubes, suggesting their binding selectivity to Pt(100) facets. The geometric matching of the molecular binding sites and the Pt(100) lattice is believed to dominate the binding selectivity. Learning from the Pt system, we effectively designed and identified Pd(111) and Pd(100) facet-specific surfactants and used them to synthesize Pd nano-octahedra and Pd nanocubes, respectively, with high yield. In this systematic study, the rationality of molecular facet-selective adsorption is demonstrated, representing a significant step toward the development of predictable nanomaterial synthesis through the design of surfactants and interfacial interactions.

■ ASSOCIATED CONTENT

Supporting Information

Additional TEM, HRTEM images and shape distributions of synthesized nanocrystals; UV−visible spectra of hydroquinone-Pt nanocrystals; geometric matching of molecular structures on metal surfaces; the energies of HOMO of molecules and work function of metal surfaces. This material is available free of charge via the Internet at http://pubs.acs.org.

■ AUTHOR INFORMATION

Corresponding Author

yhuang@seas.ucla.edu

Notes

The authors declare no competing financial interest.

■ ACKNOWLEDGMENTS

C.-Y.C., H.W., H.Z., and Y.H. acknowledge support from the Office of Naval Research (ONR) (award N00014-08-1-0985), the Army Research Office (ARO) (award 54709- MS-PCS), and the Sloan Research Fellowship. C.-Y.C. and Y.H. also acknowledge the Electron Imaging Center of Nanomachines for TEM support and B.D. for Raman spectroscopy support. V.O. acknowledges support from the U.S. Department of Energy, Office of Science, Basic Energy Sciences, under grant No. DE-FG02-07ER46433. Authors acknowledge use of computational resources of the National Energy Research Scientific Computing Center (NERSC), which is supported by the Office of Science of the U.S. Department of Energy under contract no. DE-AC02-05CH11231.

■ REFERENCES

(1) Xia, Y.; Xiong, Y.; Lim, B.; Skrabalak, S. E. *Angew. Chem., Int. Ed.* **2009**, *48*, 60−103.

(2) Anker, J. N.; Hall, W. P.; Lyandres, O.; Shah, N. C.; Zhao, J.; Van Duyne, R. P. *Nat. Mater.* **2008**, *7*, 442−453.

(3) Tao, A.; Sinsermsuksakul, P.; Yang, P. *Angew. Chem., Int. Ed.* **2006**, *45*, 4597−4601.

(4) Lim, B.; Jiang, M.; Camargo, P. H. C.; Cho, E. C.; Tao, J.; Lu, X.; Zhu, Y.; Xia, Y. *Science* **2009**, *324*, 1302−1305.

(5) Tian, N.; Zhou, Z.-Y.; Sun, S.-G.; Ding, Y.; Wang, Z. L. *Science* **2007**, *316*, 732−735.

(6) Yin, Y.; Alivisatos, A. P. *Nature* **2005**, *437*, 664−670.

(7) Zhang, Q.; Li, N.; Goebl, J.; Lu, Z.; Yin, Y. *J. Am. Chem. Soc.* **2011**, *133*, 18931−18939.

(8) Sun, Y.; Xia, Y. *Science* **2002**, *298*, 2176−2179.

(9) Ahmadi, T. S.; Wang, Z. L.; Green, T. C.; Henglein, A.; El-Sayed, M. A. *Science* **1996**, *272*, 1924−1925.

(10) Sau, T. K.; Murphy, C. J. *J. Am. Chem. Soc.* **2004**, *126*, 8648−8649.

(11) Al-Saidi, W. A.; Feng, H.; Fichthorn, K. A. *Nano Lett.* **2012**, *12*, 997−1001.

(12) Kwon, S. G.; Krylova, G.; Sumer, A.; Schwartz, M. M.; Bunel, E. E.; Marshall, C. L.; Chattopadhyay, S.; Lee, B.; Jellinek, J.; Shevchenko, E. V. *Nano Lett.* **2012**, *12*, 5382−5388.

(13) Liu, J.; Tanaka, T.; Sivula, K.; Alivisatos, A. P.; Fréchet, J. M. J. *J. Am. Chem. Soc.* **2004**, *126*, 6550−6551.

(14) Tao, A.; Sinsermsuksakul, P.; Yang, P. *Nat. Nanotechnol.* **2007**, *2*, 435−440.

(15) Jones, M. R.; Macfarlane, R. J.; Lee, B.; Zhang, J.; Young, K. L.; Senesi, A. J.; Mirkin, C. A. *Nat. Mater.* **2010**, *9*, 913−917.

(16) Cho, K.-S.; Talapin, D. V.; Gaschler, W.; Murray, C. B. *J. Am. Chem. Soc.* **2005**, *127*, 7140−7147.

(17) Chiu, C.-Y.; Li, Y.; Ruan, L.; Ye, X.; Murray, C. B.; Huang, Y. *Nat. Chem.* **2011**, *3*, 393−399.

(18) Ruan, L.; Ramezani-Dakhel, H.; Chiu, C.-Y.; Zhu, E.; Li, Y.; Heinz, H.; Huang, Y. *Nano Lett.* **2013**, *13*, 840−846.

(19) Morin, C.; Simon, D.; Sautet, P. *J. Phys. Chem. B* **2003**, *107*, 2995−3002.

(20) Saeys, M.; Reyniers, M.-F. o.; Marin, G. B.; Neurock, M. *J. Phys. Chem B* **2002**, *106*, 7489−7498.

(21) Morin, C.; Simon, D.; Sautet, P. *J. Phys. Chem. B* **2004**, *108*, 5653−5665 3097−3101.

(22) Anderson, A. B.; McDevitt, M. R.; Urbach, F. L. *Surf. Sci.* **1984**, *146*, 80−92.

(23) Mecozzi, S.; West, A. P.; Dougherty, D. A. *Proc. Natl. Acad. Sci. U.S.A.* **1996**, *93*, 10566−10571.

(24) Politzer, P.; Abrahmsen, L.; Sjoberg, P. *J. Am. Chem. Soc.* **1984**, *106*, 855−860.

(25) Kilin, D. S.; Prezhdo, O. V.; Xia, Y. *Chem. Phys. Lett.* **2008**, *458*, 113−116.

(26) Wegner, D.; Yamachika, R.; Wang, Y.; Brar, V. W.; Bartlett, B. M.; Long, J. R.; Crommie, M. F. *Nano Lett.* **2007**, *8*, 131−135.

(27) *Spartan '06*; Wavefunction Inc.: Irvine, CA, 2006.

(28) Koel, B. E.; Crowell, J. E.; Mate, C. M.; Somorjai, G. A. *J. Phys. Chem.* **1984**, *88*, 1988−1996.

(29) Queiroz, A. N.; Gomes, B. A. Q.; Moraes, W. M., Jr.; Borges, R. S. *Eur. J. Med. Chem.* **2009**, *44*, 1644−1649.

(30) Derry, G. N.; Ji-Zhong, Z. *Phys. Rev. B* **1989**, *39*, 1940−1941.

(31) Nieuwenhuys, B. E.; Sachtler, W. M. H. *Surf. Sci.* **1973**, *34*, 317−336.

(32) Lin, D.; Xing, B. *Environ. Sci. Technol.* **2008**, *42*, 7254−7259.

(33) Myers, A. K.; Benziger, J. B. *Langmuir* **1989**, *5*, 1270−1288.

(34) Soriaga, M. P.; Hubbard, A. T. *J. Am. Chem. Soc.* **1982**, *104*, 2735−2742.

(35) Lee, Y.; Park, T. G. *Langmuir* **2011**, *27*, 2965−2971.

(36) Lien, E. J.; Ren, S.; Bui, H.-H.; Wang, R. *Free Radicals Biol. Med.* **1999**, *26*, 285−294.

(37) Guibal, E.; Vincent, T.; Touraud, E.; Colombo, S.; Ferguson, A. *J. Appl. Polym. Sci.* **2006**, *100*, 3034−3043.

(38) Ford, D. C.; Xu, Y.; Mavrikakis, M. *Surf. Sci.* **2005**, *587*, 159−174.

(39) Stern, D. A.; Salaita, G. N.; Lu, F.; McCargar, J. W.; Batina, N.; Frank, D. G.; Laguren-Davidson, L.; Lin, C. H.; Walton, N. *Langmuir* **1988**, *4*, 711−722.

(40) Kahn, B. E.; Chaffins, S. A.; Gui, J. Y.; Lu, F.; Stern, D. A.; Hubbard, A. T. *Chem. Phys.* **1990**, *141*, 21−39.

(41) Kubinyi, M.; Billes, F.; Grofcsik, A.; Keresztury, G. *J. Mol. Struct.* **1992**, *266*, 339−344.

(42) Gao, P.; Weaver, M. J. *J. Phys. Chem.* **1985**, *89*, 5040−5046.

(43) Liu, G.-K.; Ren, B.; Wu, D.-Y.; Duan, S.; Li, J.-F.; Yao, J.-L.; Gu, R.-A.; Tian, Z.-Q. *J. Phys. Chem. B* **2006**, *110*, 17498−17506.

(44) Borodko, Y.; Habas, S. E.; Koebel, M.; Yang, P.; Frei, H.; Somorjai, G. A. *J. Phys. Chem. B* **2006**, *110*, 23052−23059.

(45) Sun, Q.; Tripathi, G. N. R.; Schuler, R. H. *J. Phys. Chem.* **1990**, *94*, 6273−6277.

(46) Tanaka, T.; Nakajima, A.; Watanabe, A.; Ohno, T.; Ozaki, Y. *Vib. Spectrosc.* **2004**, *34*, 157−167.

(47) Palumbo, A.; d'Ischia, M.; Misuraca, G.; Prota, G. *Biochim. Biophys. Acta, Gen. Subj.* **1991**, *1073*, 85−90.

(48) Cohen, S.; Cohen, S. G. *J. Am. Chem. Soc.* **1966**, *88*, 1533−1536.

(49) Habas, S. E.; Lee, H.; Radmilovic, V.; Somorjai, G. A.; Yang, P. *Nat. Mater.* **2007**, *6*, 692−697.
(50) Steenken, S.; Neta, P. *J. Phys. Chem.* **1979**, *83*, 1134−1137.
(51) Anderson, A. B.; Awad, M. K. *J. Am. Chem. Soc.* **1985**, *107*, 7854−7857.
(52) Feng, J.; Pandey, R. B.; Berry, R. J.; Farmer, B. L.; Naik, R. R.; Heinz, H. *Soft Matter* **2011**, *7*, 2113−2120.